© The British Computer Society 2014. All rights reserved.
For Permissions, please email: journals.permissions@oup.com
Advance Access publication on 25 February 2014
doi:10.1093/comjnl/bxu008

Content-Based Image Retrieval of Axial Brain Slices Using a Novel LBP with a Ternary Encoding

Abraham Varghese[1]*, Kannan Balakrishnan[2], Reji Rajan Varghese[3] and Joseph S. Paul[4]

[1] *Computer Science and Engineering, Adi Shankara Institute of Engineering and Technology, Kalady, Ernakulam, India*
[2] *Department of Computer Applications, CUSAT, Cochin, India*
[3] *Co-operative Medical college, Cochin, India*
[4] *Indian Institute of Information Technology and Management-Kerala,Trivandrum, India*
**Corresponding author: abrahamvarghese77@gmail.com*

Retrieval of similar anatomical structures of brain MR images across patients would help the expert in diagnosis of diseases. In this paper, modified local binary pattern with ternary encoding called modified local ternary pattern (MOD-LTP) is introduced, which is more discriminant and less sensitive to noise in near-uniform regions, to locate slices belonging to the same level from the brain MR image database. The ternary encoding depends on a threshold, which is a user-specified one or calculated locally, based on the variance of the pixel intensities in each window. The variance-based local threshold makes the MOD-LTP more robust to noise and global illumination changes. The retrieval performance is shown to improve by taking region-based moment features of MOD-LTP and iteratively reweighting the moment features of MOD-LTP based on the user's feedback. The average rank obtained using iterated and weighted moment features of MOD-LTP with a local variance-based threshold, is one to two times better than rotational invariant LBP (Unay, D., Ekin, A. and Jasinschi, R.S. (2010) Local structure-based region-of-interest retrieval in brain MR images. *IEEE Trans. Inf. Technol. Biomed.*, 14, 897–903.) in retrieving the first 10 relevant images.

Keywords: content-based image retrieval; local binary pattern; modified local binary pattern; modified local ternary pattern; rotational scaling & translational invariant features

Received 7 November 2012; revised 22 October 2013
Handling editor: Ugur Halici

Downloaded from http://comjnl.oxfordjournals.org/ by guest on October 14, 2014

1. INTRODUCTION

The ever-increasing volume of images produced from different sources, the inadequacy of human language alone to describe image contents that are visually recognizable and the impracticality of manually indexing these images have led to the rise of content-based image retrieval (CBIR) techniques [1–3]. With the maturation of computing technology and the high speed processor, indexing of images can be done using features like color, texture, shape, etc. instead of key words. One of the most challenging parts of developing CBIR is extracting the salient features of images that can be used to characterize edges, textures and contours of interest. This is even more difficult with respect to the medical field, especially in brain MR images due to challenges like MR inter- and intra-patient intensity variations, misalignment of images, etc. [4, 5]. Local binary pattern (LBP) has been recently proved useful in describing medical images, which has a low computational complexity and a low sensitivity to changes in illumination. Traditional LBP is formed by taking the difference between the gray value of a pixel (g_c) and the gray values of P pixels (g_k) in a local neighborhood. The LBP has been applied in various applications like face recognition, fingerprint identification, texture classification, MR brain image retrieval, etc. [6–9]. Several variants like uniform binary pattern, elliptical binary pattern, median binary pattern, center-symmetric LBP [10–13] etc. are depicted in the literature. In order to reduce sensitivity to noise, a three-valued coding, local ternary pattern (LTP) is proposed [14]. The idea of a three-valued coding is proposed also in [5, 16], where a fuzzy thresholding function is used to make the LBP operator more robust to noise. In this paper, a variant of LBP, modified local ternary pattern (MOD-LTP), which is more discriminant and less sensitive to noise in the uniform or near-uniform regions, is introduced as a texture descriptor for brain MR image retrieval. MOD-LTP is a better texture descriptor as it captures information from every pixel in the local neighborhood. A comparison has been made with traditional LBP as well as MOD-LBP in terms of accuracy of retrieval and sensitivity to noise.

2. METHODOLOGY

The overview of the image retrieval scheme is shown in Fig. 1. MOD-LTP is computed using a window of size w. The normalized histogram of the resultant image is taken as feature vectors for similarity computation. The images in the database are ranked based on the Bhattacharya distance between query and database images. The average rank and accuracy for a set of query images to locate similar images are calculated. The moment features of MOD-LTP are computed spatially over an angularly partitioned area and performance of the retrieval system is evaluated using the distance function of moment features. To achieve an optimum performance, the moment features of MOD-LTP are reweighted based on the relevance of individual features in the retrieval process.

2.1. Local binary pattern, modified local binary pattern and modified local ternary pattern

LBP is formed by taking the difference between the gray value of a pixel (g_c) and the gray values of P pixels (g_i) in a local neighborhood.

$$\mathrm{LBP} = \sum_{i=0}^{P-1} s(g_i - g_c)2^i, \quad \begin{Bmatrix} s(x) = 1,\ x \geq 0 \\ 0,\ x < 0 \end{Bmatrix}. \qquad (1)$$

Here, a P-bit binary number is multiplied by a power of 2 to get an LBP code. LBP around a circular neighborhood with P pixels and radius R is denoted as $\mathrm{LBP}_{P,R}$ in which the coordinates of the neighborhood pixels, $g_{i,}(i = 0, 1, 2, \ldots, P-1)$ around the center pixel $g_c(x_c, y_c)$ are $(x_c + R\cos(2\pi i/P),\ y_c - R\sin(2\pi i/P))$. The gray values of the neighboring pixels that are not in the image grids can be estimated using bilinear interpolation. The signs of the differences obtained using Equation (1) in a neighborhood are interpreted as a P-bit binary number, resulting in 2^P distinct values in the LBP code. One way to eliminate the effect of rotation is to perform a bitwise shift operation on the binary pattern $P-1$ times and assign the smallest decimal equivalent to the central pixel which is referred to as rotational invariant LBP($\mathrm{LBP}^{ri}_{P,R}$). We refer to $\mathrm{LBP}^{riu2}_{P,R}$ as rotational invariant LBP with a limited number of transitions [13].

LBP has been proved to be invariant to monotonic gray scale changes, intensity inhomogeneity, etc. [17], but it is sensitive to noise and ignores the magnitude of gray level differences. The definition of the LBP is modified by incorporating gray scale information as

$$\mathrm{MOD-LBP} = \frac{1}{P}\sum_{i=0}^{P-1} s(g_i - g_c)(g_i - \mu)^2, \qquad (2)$$

where μ is the mean of the P neighborhood pixels and $\left(s(x) = \begin{matrix} 1, x \geq 0 \\ 0, x < 0 \end{matrix}\right)$ [18]. In MOD-LBP, the weight assigned to each binary number in the neighborhood is the squared difference between intensity of that pixel and the mean intensity of the neighboring pixels. To make it robust to noise in the uniform or near-uniform region, P-bit binary pattern is generated using a three-value encoding, based on a global as well as a local threshold σ. The ternary pattern so obtained is split into two binary patterns in which the first binary pattern is obtained by considering positive components and making the negative component zero. The second binary pattern is obtained by considering the negative components and making the positive components as zero. The resultant binary pattern is obtained by concatenating the two binary patterns. The resultant image formed by assigning the real number equivalent of the weighted binary number to the central pixel is termed as MOD-LTP and is given in Equation (3).

$$\begin{aligned} &\mathrm{MOD\text{-}LTP} = \frac{1}{P}\sum_{i=0}^{P-1} s(g_i - g_c)(g_i - \mu)^2, \\ &\text{where} \quad s(g_i - g_c) = \begin{matrix} 1, g_i - g_c > \sigma, \\ 0, |g_i - g_c| \leq \sigma, \\ -1, g_i - g_c < -\sigma. \end{matrix} \end{aligned} \qquad (3)$$

In traditional LTP, the threshold is calculated globally, which is sensitive to global illumination changes. In MOD-LTP, the threshold is chosen locally based on the variance of the pixel intensities of the neighboring pixels in addition to the user-specified value. Since the threshold is based on the local variance and the MRI is locally smooth, it is invariant to monotonic gray-level change and it can resist intra-image illumination as long as absolute gray-scale values are not much affected. As every pixel in the local neighborhood is involved in the MOD-LTP computation, the method is invariant to some basic geometric transformations and intensity variations with respect to that neighborhood. The robustness of the local measure to handle intensity-related problems is shown in the result session. The pixel numbering of the neighborhoods of size 3 and 5 used in the LBP and MOD-LTP computation are shown in Fig. 2.

2.2. Moment invariants

A suitable threshold on MOD-LBP captures boundaries of some structures that the human visual system tends to use

Downloaded from http://comjnl.oxfordjournals.org/ by guest on October 14, 2014

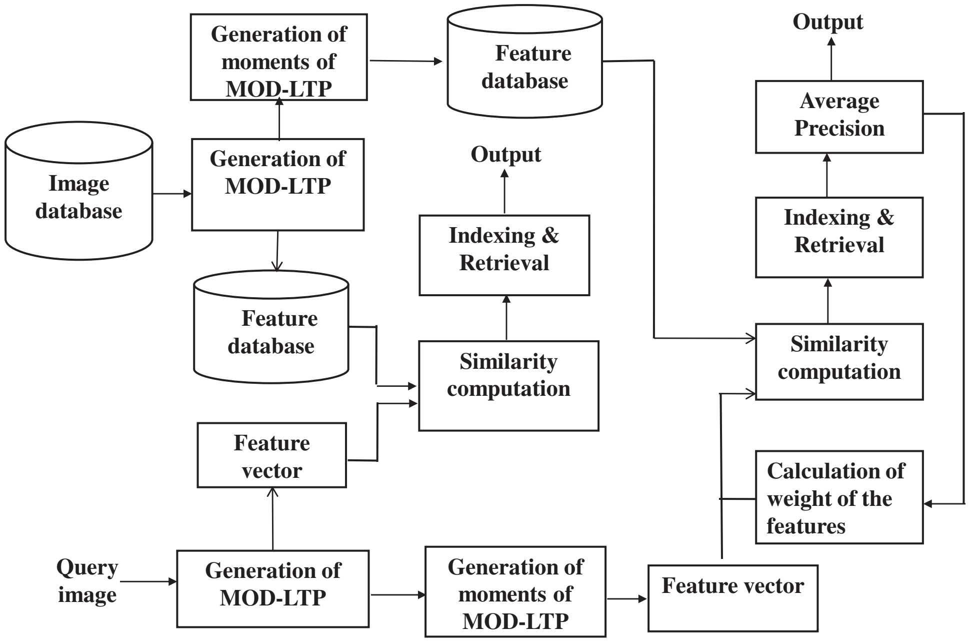

FIGURE 1. Block diagram of image retrieval scheme.

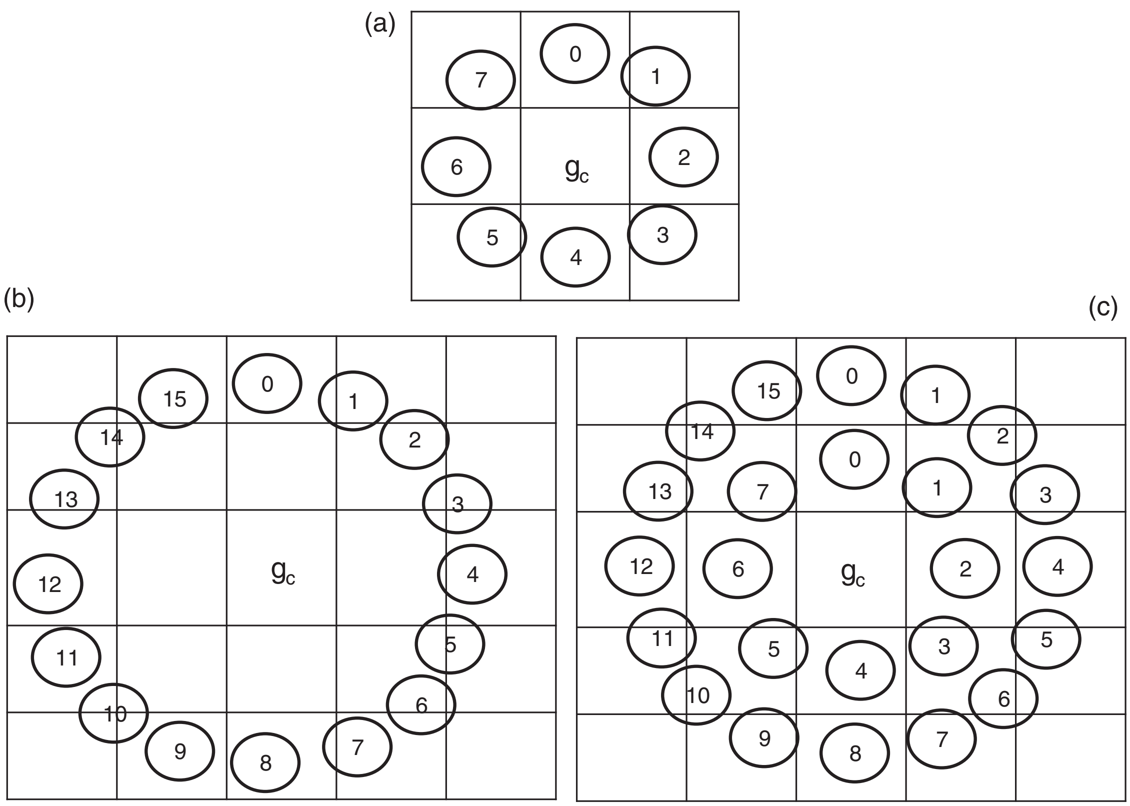

FIGURE 2. Pixel numbering of neighborhood pixels (**a**) for LBP and MOD-LTP computation with window size 3 (**b**) for LBP computation with window size 5 (**c**) for MOD-LTP computation with windowsize 5.

Downloaded from http://comjnl.oxfordjournals.org/ by guest on October 14, 2014

in identification. The region-based moment features, which is invariant to translation and scaling, obtained from MOD-LTP is used as features for computing similarity between images. These features that are invariant to translation and rotation have proved to be the most useful because of the variability in the orientation of anatomical regions within the brain across subjects. Two-dimensional moments of order $(p+q)$ for digital image $f(x, y)$ is defined to be

$$m_{pq} = \sum_p \sum_q x^p y^q f(x, y), \tag{4}$$

where, $p, q = 0, 1, 2$, etc. [19]. To attain a Translation Invariant measure, raw moments are replaced by central moments, which is defined as

$$\mu_{pq} = \sum \sum (x - \bar{x})^p (y - \bar{y})^q f(x, y), \tag{5}$$

where $\bar{x} = m_{10}/m_{00}$, $\bar{y} = m_{01}/m_{00}$.

The scaling invariant may be obtained by further normalizing μ_{pq} as

$$\eta_{pq} = \mu_{00}^{\mu_{pq}/((p+q)/2+1)}. \tag{6}$$

Using this, a set of seven rotational scaling & translational invariant features (RST) is derived by Schalkoff [20]. The relative difference in magnitude of the eigenvalues is thus an indication of the eccentricity of the image, or how elongated it is. The eccentricity is $\sqrt{1 - \lambda_2/\lambda_1}$, where λ_1, λ_2 are the eigenvalues of the co-variance matrix. We have used central moments, RST features and eccentricity for image comparison.

2.3. Feature extraction

The MOD-LTP is computed using Equation (3) and the pixel value of MOD-LTP is brought into the range of integer values $[0\ L_1]$. Normalized histogram of resultant images is taken as feature vectors and the Bhattacharya distance is used for defining similarity between the query image and database images. To preserve similarity attributes between anatomical similar structures of the query slice, and member slices from the database, we make use of the fact that brain slices are quasi-symmetric across the left and right hemispheres. In the sequel, we extract moment features of MOD-LTP over an angularly partitioned grid with respect to a reference line (line with respect to which 2D brain image exhibits maximum symmetry). The central moments of orders 1–25, eigenvalues of the central moments, RST features [19] obtained from the central moments and the eccentricity are calculated for each partitioned grid. For m features defined at n spatial locations, the LBP image is represented using a collection of m spatial vectors, each of size $n \times 1$. For a query image Q, we define the feature matrix to be

$$F^q = \begin{bmatrix} f^q(1,1) & f^q(1,2) & \dots & f^q(1,m) \\ f^q(2,1) & f^q(2,2) & \dots & f^q(2,m) \\ \vdots & \vdots & & \vdots \\ f^q(n,1) & f^q(n,2) & \dots & f^q(n,m) \end{bmatrix}$$

and the feature matrix of the database images as

$$F_i^I = \begin{bmatrix} f_i^I(1,1) & f_i^I(1,2) & \dots & f_i^I(1,m) \\ f_i^I(2,1) & f_i^I(2,2) & \dots & f_i^I(2,m) \\ \vdots & \vdots & & \vdots \\ f_i^I(n,1) & f_i^I(n,2) & \dots & f_i^I(n,m) \end{bmatrix},$$
$$i = 1, 2 \dots, N.$$

The distance matrix is found by calculating the distance between feature vectors of the query image F^q and those in the database using the Euclidean distance function. The entries in the distance matrix correspond to different features and may vary within a wide range. To ensure equal emphasis for all vectors, entries in the distance matrix are brought into the range $[-1\ \ 1]$. The distance value between the query and the ith image in the database is

$$d(I_i, Q) = \sqrt{\sum_{j=1}^{m} \sum_{k=1}^{n} (\mathrm{F^q}(k, j) - F_i^I(k, j))^2}. \tag{7}$$

This distance value vector so obtained is arranged in ascending order and Precision-Recall is then calculated.

2.4. Reweighting the features

As one visual feature is not sufficient to describe different aspects of the image content, multiple features are required to characterize the content of images. The basic method uses equal weights on the assumption that different features have the same importance in the process of retrieval. But in most cases, they do not have the same importance. The impact of certain features is very low compared with other features. Therefore, it is absolutely necessary to find the impact of the individual features on the retrieval process to get a better result. To get a higher system performance, methods for multiple features combination are proposed [20, 21]. The general idea is to assign higher weights to a feature that is more important for the query image. In order to observe the effect of an individual feature, a single feature aggregation distance measure (SFAD) between the query and the ith image in the database using the jth feature,

$$d^{(j)}(I_i, Q) = \sqrt{\sum_{k=1}^{n} (\mathrm{F^q}(k, j) - F_i^I(k, j))^2},$$
$$j = 1, 2 \dots, m \text{ is calculated.}$$

The corresponding distance vector between the query image Q and N images in the database using the jth feature is $D^{(j)}(Q) = [d^{(j)}(I_1, Q), d^{(j)}(I_2, Q) \dots d^{(j)}(I_N, Q)]$. We arrange the distance vector in ascending order and corresponding indices of the images in the database are found out. In accordance with these indices, the images in the database are arranged as $I_R^{(j)} = [I_{r_1}^{(j)}, I_{r_2}^{(j)}, \dots, I_{r_N}^{(j)}]$ called the retrieved set.

Downloaded from http://comjnl.oxfordjournals.org/ by guest on October 14, 2014

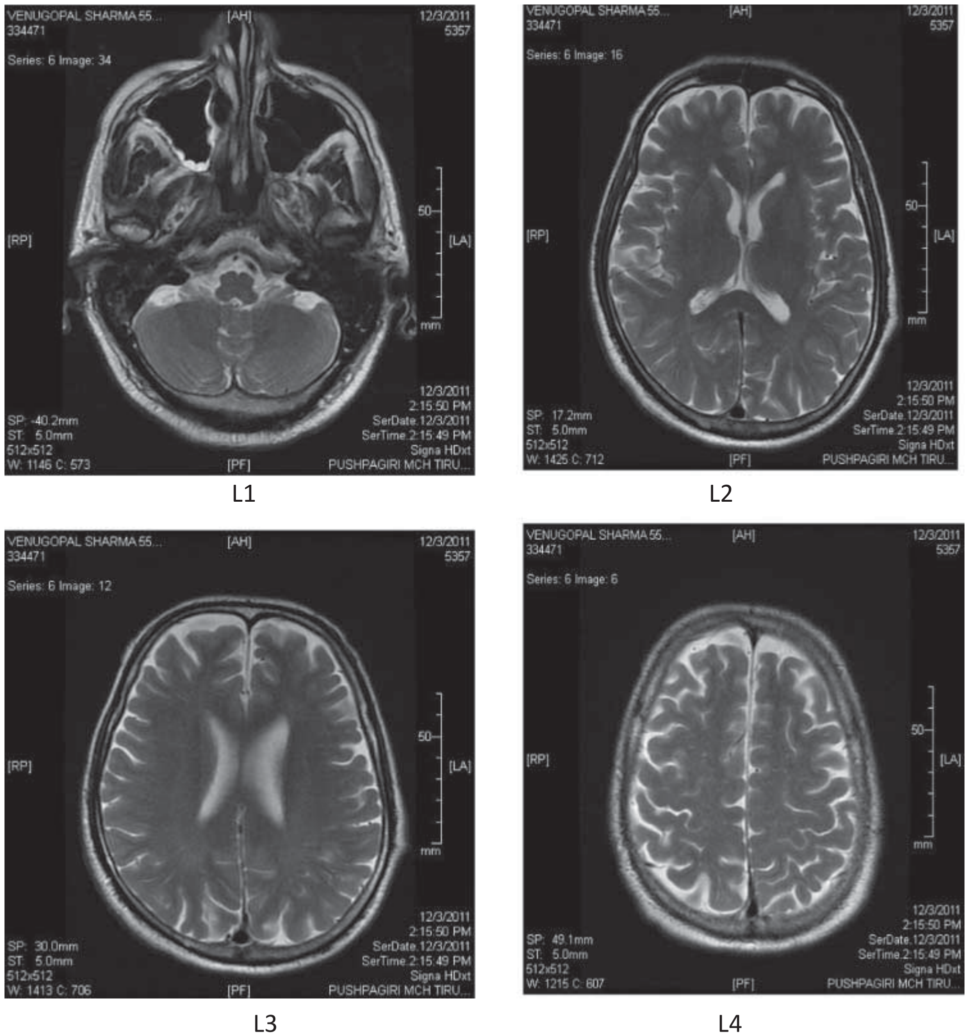

FIGURE 3. Different classes of T2-weighted axial MR slices.

We define the retrieval index (RI): n_l to be the number of images to be traversed in the retrieved set to encounter the lth relevant image, $l = 1, 2 \ldots, L$ corresponds to the given query. The precision for the lth relevant image is defined as

$$P_{n_l}^{(j)} = \frac{l}{n_l}. \tag{8}$$

The recall of the lth relevant image is defined as

$$R_{n_l}^{(j)} = \frac{l}{L}. \tag{9}$$

Therefore, the precision and recall of query image Q using the jth feature is $P^{(j)}(Q) = \left[P_{n1}^{(j)}, P_{n2}^{(j)}, \ldots, P_{n_L}^{(j)}\right]$, $P_{n1}^{(j)} > P_{n2}^{(j)} > \cdots > P_{n_L}^{(j)}$ and $R^{(j)}(Q) = [R_{n1}^{(j)}, R_{n2}^{(j)}, \ldots, R_{n_L}^{(j)}]$. Consequently, the average precision based on the jth feature is $AvgP^{(j)} = \frac{\sum_{l=1}^{L} P_{n_l}^{(j)}}{L}$, $j = 1, 2, \ldots, m$. The features having higher value of $AvgP^{(j)}$ will have a more dominant role in retrieving the relevant images. Hence it is appropriate to weigh each feature vector based on the respective $AvgP^{(j)}$ value prior to calculating the distance matrix. Based on the value of $AvgP^{(j)}$, each feature will be given a weight and new average precision, $AvgP$ is calculated by integrating m features. This repeats and new average precision $AvgP$ is calculated each time till it attains an optimum value.

3. PERFORMANCE EVALUATION

3.1. Average rank and accuracy

For a set of queries, the average rank and accuracy of the retrieval is calculated based on the images retrieved. If the

Downloaded from http://comjnl.oxfordjournals.org/ by guest on October 14, 2014

relevant images are in a succeeding order without the absence of irrelevant images in between, the corresponding query image is assigned a rank of 1. An ideal retrieval algorithm will therefore yield a rank of 1 for all the Q query images. In practice, however, each of the Q query images will get a different rank depending upon the number of images retrieved. An average rank, which shows the closeness of the system performance, is calculated using the formula

$$\text{Average rank} = \frac{1}{N_R}\left(\sum_{i=1}^{N_R} R_i - \frac{N_R(N_R-1)}{2}\right), \tag{10}$$

TABLE 1. The dissimilarity score between original and degraded images.

Method	Window size	Bias field 20%	Bias field 40%
Histogram		1.28×10^{-1}	1.3×10^{-1}
LBP(8,1)	3	2.6×10^{-3}	4.1×10^{-3}
MOD-LBP(8,1)	3	2×10^{-3}	2.6×10^{-3}
MOD-LTP(8,1)	3	1.8×10^{-3}	2.1×10^{-3}

where N_R represents the number of relevant images and R_i represents the rank at which the ith relevant image is retrieved [22].

The accuracy of the retrieval system for a set of queries is also calculated using the formula

$$\text{Acc} = \left(1 - \frac{\text{No of irrelevant images retrieved}}{\text{Total no of irrelevant images}}\right) \times 100, \tag{11}$$

In the results section, we will illustrate how the average ranking and accuracy are made use of in classifying the retrieval performance at different levels.

4. RESULTS

The experiment is performed on T1 and T2 weighted clinical datasets as well as the Brainweb simulated database (http://www.bic.mni.mcgill.ca/brainweb).

The slices (T2 weighted) used in this work were acquired on a 1.5 Tesla, General Electric (GE)—Signa HDxt MR Scanner from Pushpagiri Medical College Hospital, Tiruvalla, Kerala, India. Axial, 2D, 5 mm thick slice images, with a slice gap of 1.5 mm were acquired with the field of view (FOV) of range 220

TABLE 2. The average rank of retrieving the first six relevant images using the histogram of different LBP variants.

LBP variants	Levels	Measure	Number of relevant images retrieved 1	2	3	4	5
LBP (window size 3)	L1	Average Rank	1.11	1.61	2.26	3.03	3.73
		Accuracy %	99.92	99.21	98.19	96.93	96.06
	L2	Average Rank	1.13	1.20	1.29	1.33	1.36
		Accuracy %	99.90	99.80	99.65	99.65	99.65
	L3	Average Rank	1.46	1.54	1.77	2.29	2.78
		Accuracy %	99.66	99.55	99.10	97.92	97.25
	L4	Average Rank	1.31	1.34	1.40	1.45	1.51
		Accuracy %	99.77	99.72	99.63	99.53	99.44
MOD-LBP (window size 3)	L1	Average Rank	2.22	2.44	2.81	3.33	3.98
		Accuracy %	99.13	98.82	98.19	97.24	96.06
	L2	Average Rank	1.07	1.20	1.36	1.47	1.59
		Accuracy %	99.95	99.75	99.51	99.41	99.21
	L3	Average Rank	1.31	1.42	1.62	1.77	1.97
		Accuracy %	99.78	99.61	99.27	99.10	98.71
	L4	Average Rank	1.19	1.31	1.35	1.42	1.50
		Accuracy %	99.86	99.67	99.67	99.53	99.39
MOD-LTP (threshold based on local variance)	L1	Average Rank	1.33	1.61	1.96	2.28	2.89
		Accuracy %	99.76	99.37	98.82	98.42	96.93
	L2	Average Rank	1.00	1.07	1.16	1.27	1.37
		Accuracy %	100.00	99.90	99.75	99.56	99.41
	L3	Average Rank	1.15	1.27	1.44	1.54	1.68
		Accuracy %	99.89	99.72	99.44	99.38	99.10
	L4	Average Rank	1.00	1.03	1.08	1.14	1.19
		Accuracy %	100.00	99.95	99.86	99.77	99.72

Downloaded from http://comjnl.oxfordjournals.org/ by guest on October 14, 2014

to 250 mm. The T2 (TR/TE (eff.) of 3500 − 4500/85 − 105 (eff.) ms) images were collected using fast spin echo (FSE) sequences with a matrix size of 320 × 224 (Frequency × Phase) and a NEX (Averages) of 2.

We have categorized brain unregistered MR images of different persons into four levels and evaluated the performance of the method (Fig. 3).

L1. The foramen magnum (The cerebellum with paranasal sinus is present).
L2. Above the fourth ventricle (Caudate nucleus, thalamus, basal ganglia are seen).
L3. Mid-ventricular section.
L4. Above the ventricle.

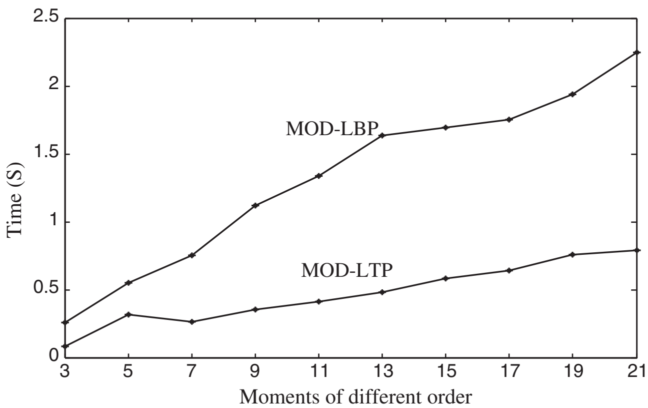

FIGURE 4. Time for calculating moments of different order.

To test the robustness of MOD-LTP with respect to intensity variations simulated bias fields from the BrainWeb MR simulator (20 and 40%) are used (http://www.bic.mni.mcgill.ca/brainweb). These bias fields provide smooth variations of intensity across the image. As the MOD-LTP is calculated locally, intensity inhomogeneity has less sensitivity to it because the bias field in an MRI is locally smooth. The degree of dissimilarity between MOD-LTP of the original and the degraded images (100 images randomly chosen) are computed using the Bhattacharyya distance, $d = 1 - \sum_{i=0}^{L1-1} \sqrt{p(i)q(i)}$, where p and q are normalized histograms with $L1$-bins. The average dissimilarity scores fall in the range of [0 1], where 0 means that all original images and their degraded images are perfectly similar. Table 1 shows the effect of the bias field in similarity computation between the original images and the degraded images. It shows that the local measure is useful in handling intensity-related problems and, in particular, MOD-LTP with a local threshold is robust to global illumination changes. As the bias field increases, the dissimilarity increases and MOD-LTP with window size 3 shows less dissimilarity compared with other variants.

The performance of the retrieval system is evaluated by choosing a set of T1-weighted BrainWeb simulated images (0% noise and 0% inhomogenetiy). The average rank and accuracy are calculated based on the histogram of different LBP variants. Table 2 illustrates the comparison of LBP, MOD-LBP and MOD-LTP in retrieving the first five relevant images. It reveals that the MOD-LTP with a window size 3 gets 100% accuracy for retrieving the first relevant image for levels L2 and L4, and 99% for L1 and L3.

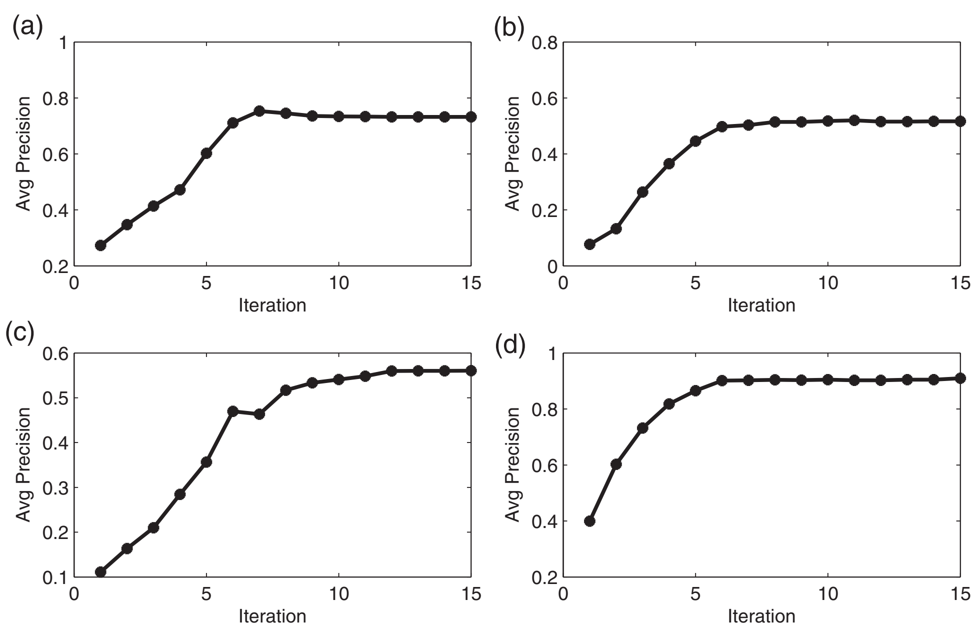

FIGURE 5. Average precision vs. iteration for (**a**) L1, (**b**) L2, (**c**) L3, (**d**) L4.

Downloaded from http://comjnl.oxfordjournals.org/ by guest on October 14, 2014

4.1. Moments of MOD-LTP

To improve the accuracy of the retrieval system, the MOD-LTP computed on the clinical dataset using Equation (3) is divided into different angularly partitioned regions. For each region, the features, central moments of orders 1–25, RST invariant features obtained from the central moments and the eccentricity are extracted as outlined in section II.C.

This identifies the boundary of the homogeneous region and it reduces the time complexity of calculating moments of higher order. Figure 4 shows the time taken for calculating moments of different orders of the MOD-LBP image and the MOD-LTP image with a threshold 0.1. As the order of the moments increases, the time complexity for extracting moments also increases. The rate at which the time increases is less in MOD-LTP when compared with MOD-LBP. It is shown that the

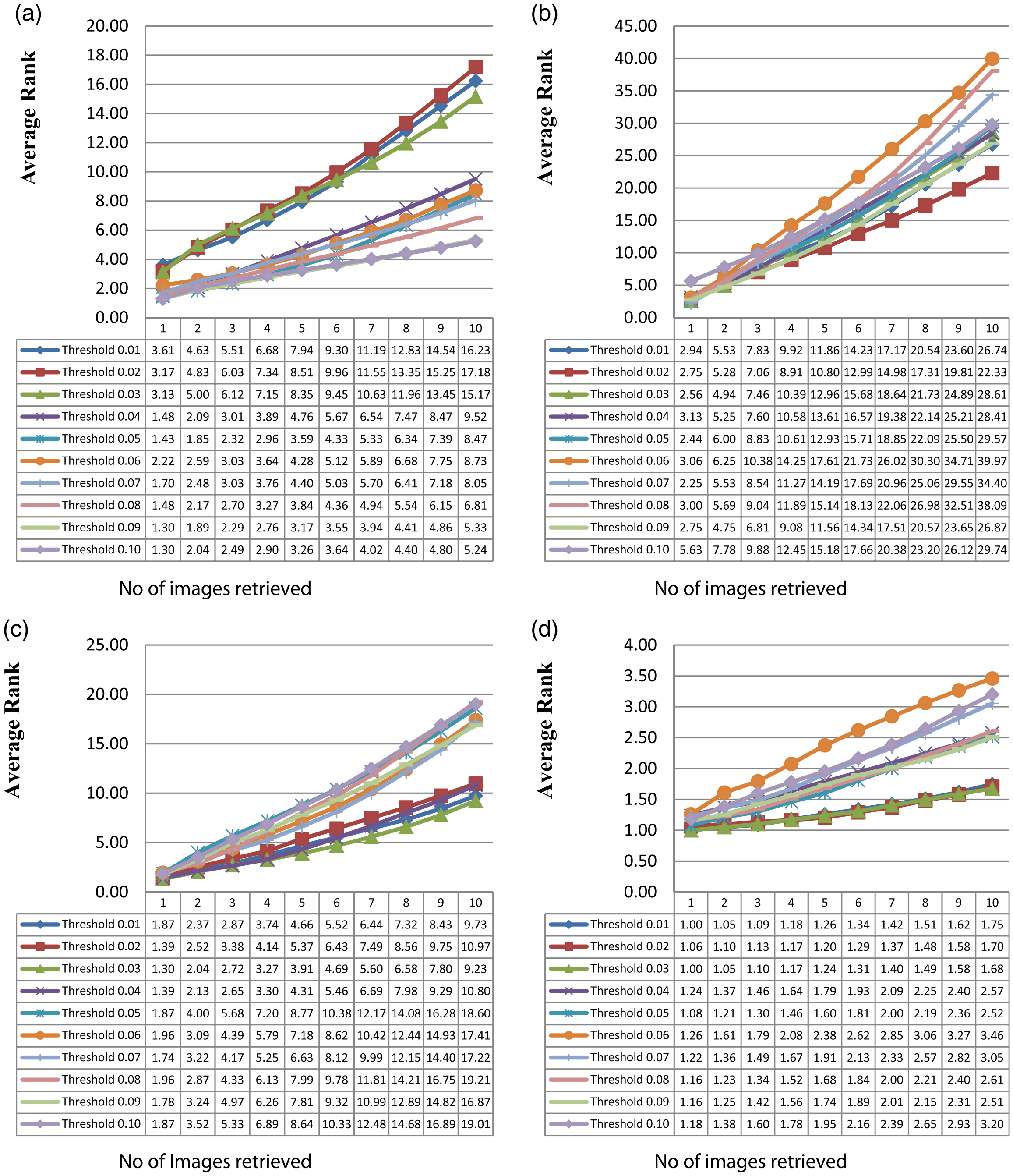

(a)

	1	2	3	4	5	6	7	8	9	10
Threshold 0.01	3.61	4.63	5.51	6.68	7.94	9.30	11.19	12.83	14.54	16.23
Threshold 0.02	3.17	4.83	6.03	7.34	8.51	9.96	11.55	13.35	15.25	17.18
Threshold 0.03	3.13	5.00	6.12	7.15	8.35	9.45	10.63	11.96	13.45	15.17
Threshold 0.04	1.48	2.09	3.01	3.89	4.76	5.67	6.54	7.47	8.47	9.52
Threshold 0.05	1.43	1.85	2.32	2.96	3.59	4.33	5.33	6.34	7.39	8.47
Threshold 0.06	2.22	2.59	3.03	3.64	4.28	5.12	5.89	6.68	7.75	8.73
Threshold 0.07	1.70	2.48	3.03	3.76	4.40	5.03	5.70	6.41	7.18	8.05
Threshold 0.08	1.48	2.17	2.70	3.27	3.84	4.36	4.94	5.54	6.15	6.81
Threshold 0.09	1.30	1.89	2.29	2.76	3.17	3.55	3.94	4.41	4.86	5.33
Threshold 0.10	1.30	2.04	2.49	2.90	3.26	3.64	4.02	4.40	4.80	5.24

(b)

	1	2	3	4	5	6	7	8	9	10
Threshold 0.01	2.94	5.53	7.83	9.92	11.86	14.23	17.17	20.54	23.60	26.74
Threshold 0.02	2.75	5.28	7.06	8.91	10.80	12.99	14.98	17.31	19.81	22.33
Threshold 0.03	2.56	4.94	7.46	10.39	12.96	15.68	18.64	21.73	24.89	28.61
Threshold 0.04	3.13	5.25	7.60	10.58	13.61	16.57	19.38	22.14	25.21	28.41
Threshold 0.05	2.44	6.00	8.83	10.61	12.93	15.71	18.85	22.09	25.50	29.57
Threshold 0.06	3.06	6.25	10.38	14.25	17.61	21.73	26.02	30.30	34.71	39.97
Threshold 0.07	2.25	5.53	8.54	11.27	14.19	17.69	20.96	25.06	29.55	34.40
Threshold 0.08	3.00	5.69	9.04	11.89	15.14	18.13	22.06	26.98	32.51	38.09
Threshold 0.09	2.75	4.75	6.81	9.08	11.56	14.34	17.51	20.57	23.65	26.87
Threshold 0.10	5.63	7.78	9.88	12.45	15.18	17.66	20.38	23.20	26.12	29.74

(c)

	1	2	3	4	5	6	7	8	9	10
Threshold 0.01	1.87	2.37	2.87	3.74	4.66	5.52	6.44	7.32	8.43	9.73
Threshold 0.02	1.39	2.52	3.38	4.14	5.37	6.43	7.49	8.56	9.75	10.97
Threshold 0.03	1.30	2.04	2.72	3.27	3.91	4.69	5.60	6.58	7.80	9.23
Threshold 0.04	1.39	2.13	2.65	3.30	4.31	5.46	6.69	7.98	9.29	10.80
Threshold 0.05	1.87	4.00	5.68	7.20	8.77	10.38	12.17	14.08	16.28	18.60
Threshold 0.06	1.96	3.09	4.39	5.79	7.18	8.62	10.42	12.44	14.93	17.41
Threshold 0.07	1.74	3.22	4.17	5.25	6.63	8.12	9.99	12.15	14.40	17.22
Threshold 0.08	1.96	2.87	4.33	6.13	7.99	9.78	11.81	14.21	16.75	19.21
Threshold 0.09	1.78	3.24	4.97	6.26	7.81	9.32	10.99	12.89	14.82	16.87
Threshold 0.10	1.87	3.52	5.33	6.89	8.64	10.33	12.48	14.68	16.89	19.01

(d)

	1	2	3	4	5	6	7	8	9	10
Threshold 0.01	1.00	1.05	1.09	1.18	1.26	1.34	1.42	1.51	1.62	1.75
Threshold 0.02	1.06	1.10	1.13	1.17	1.20	1.29	1.37	1.48	1.58	1.70
Threshold 0.03	1.00	1.05	1.10	1.17	1.24	1.31	1.40	1.49	1.58	1.68
Threshold 0.04	1.24	1.37	1.46	1.64	1.79	1.93	2.09	2.25	2.40	2.57
Threshold 0.05	1.08	1.21	1.30	1.46	1.60	1.81	2.00	2.19	2.36	2.52
Threshold 0.06	1.26	1.61	1.79	2.08	2.38	2.62	2.85	3.06	3.27	3.46
Threshold 0.07	1.22	1.36	1.49	1.67	1.91	2.13	2.33	2.57	2.82	3.05
Threshold 0.08	1.16	1.23	1.34	1.52	1.68	1.84	2.00	2.21	2.40	2.61
Threshold 0.09	1.16	1.25	1.42	1.56	1.74	1.89	2.01	2.15	2.31	2.51
Threshold 0.10	1.18	1.38	1.60	1.78	1.95	2.16	2.39	2.65	2.93	3.20

FIGURE 6. The average rank of set of queries with different threshold in each classes. (**a**) L1, (**b**) L2, (**c**) L3, (**d**) L4.

Downloaded from http://comjnl.oxfordjournals.org/ by guest on October 14, 2014

TABLE 3. The comparison of different LBP variants in terms of average rank in retrieving first 10 relevant images.

		Number of relevant images retrieved									
Class	Method	1	2	3	4	5	6	7	8	9	10
L1	$LBP^{ri}_{P,R}$ [5]	2.47	5.3	6.82	8.53	10.1	11.5	13.1	15.33	18.01	20.9
	$LBP^{riu2}_{P,R}$	2.53	5.53	7.06	8.66	10.2	11.8	13.7	15.77	17.86	20
	Histogram of MOD-LBP	2.73	3.36	4.04	5.06	6.32	7.75	9.29	11	12.85	14.91
	Weighted Moments of MOD-LBP	1.48	2.09	3.01	3.89	4.76	5.67	6.54	7.47	8.47	9.52
	Weighted Moments of MOD-LTP (threshold 0.12)	1.17	1.93	2.28	2.65	3.09	3.49	3.84	4.19	4.54	4.93
	Weighted Moments of MOD-LTP (local variance based threshold)	1.43	1.85	2.45	3.04	3.63	4.33	5.11	5.94	6.84	8.9
L2	$LBP^{ri}_{P,R}$ [5]	1.56	2.97	3.73	4.55	5.35	6.03	6.71	7.39	8.15	9.11
	$LBP^{riu2}_{P,R}$	1.81	2.40	3.16	3.87	4.48	5.08	5.76	6.67	7.63	8.58
	Histogram of MOD-LBP	1.69	3.09	3.81	4.50	5.20	5.86	6.55	7.15	7.95	8.79
	Weighted Moments of MOD-LBP	1.63	2.75	3.54	4.19	4.80	5.45	6.16	6.91	7.69	8.56
	Weighted Moments of MOD-LTP (threshold 0.12)	1.87	2	2.39	2.79	3.23	3.70	4.26	4.88	5.51	6.16
	Weighted Moments of MOD-LTP (local variance based threshold)	1.68	2.06	2.60	3.10	3.47	4.01	4.63	5.52	6.64	8.08
L3	$LBP^{ri}_{P,R}$ [5]	5.8	6.86	7.91	9.45	10.8	12.6	14.5	16.63	19.01	21.69
	$LBP^{riu2}_{P,R}$	7.26	8.03	9.08	10.4	11.6	12.8	14.1	16.03	18.01	20.26
	Histogram of MOD-LBP	3.73	4.73	5.88	7.05	8.28	9.55	11.1	12.69	14.45	16.52
	Weighted Moments of MOD-LBP	1.52	2.20	3.01	3.93	5.14	6.33	7.49	8.72	9.98	11.30
	Weighted Moments of MOD-LTP (threshold 0.12)	1.87	2.37	2.87	3.74	4.66	5.52	6.44	7.32	8.43	9.73
	Weighted Moments of MOD-LTP (local variance based threshold)	1.83	2.39	2.96	3.80	4.77	5.88	7.01	8.24	9.58	11.16
L4	$LBP^{ri}_{P,R}$ [5]	1.64	1.95	2.26	2.54	2.81	3.10	3.40	3.72	4.05	4.38
	$LBP^{riu2}_{P,R}$	1.59	1.86	2.05	2.22	2.42	2.61	2.83	3.07	3.34	3.62
	Histogram of MOD-LBP	1.32	1.55	1.70	1.83	1.98	2.14	2.30	2.46	2.65	2.85
	Weighted Moments of MOD-LBP	1.06	1.13	1.23	1.34	1.44	1.56	1.68	1.84	1.99	2.15
	Weighted Moments of MOD-LTP (threshold 0.12)	1.00	1.05	1.09	1.18	1.26	1.34	1.42	1.51	1.62	1.75
	Weighted Moments of MOD-LTP (local variance based threshold)	1.48	1.57	1.65	1.76	1.87	2.01	2.16	2.37	2.58	2.79

time taken for extracting moments of order 21 using MOD-LTP is 0.6 s, while that of MOD-LBP is 2.3 s. The similarity between the query and the target is computed using a Euclidean distance measure based on individual features. It is observed that each of the 34 features listed exhibits a varying degree of performance with reference to the average rank. Since the presence of some features degrades the overall performance of the retrieval, we reweighted the features based on the reweighting procedure. Figure 5 shows the average precision of randomly chosen images in each class after applying the reweighting algorithm. It is observed that the average precision increases from 25 to 90% in L1, 22 to 48% in L2, 30 to 55% in L3 and 50 to 90% in L4.

Figure 6 shows the average rank of different level images based on various thresholds. It shows a better average rank which corresponds to a threshold of 0.1 in L1, 0.02 in L2, and 0.03 in L3 and L4.

Table 3 gives the comparison between various LBP variants in retrieving the first 10 relevant images in terms of average rank. Histogram-based MOD-LBP performs better than LBP [5]. The moment invariant features extracted from the angularly partitioned grid of MOD-LTP improve the performance of the retrieval system. A further improvement is achieved by reweighting the moment features of MOD-LTP on proper choice of the threshold and a local variance-based threshold.

The top five images retrieved corresponds to a randomly chosen image in each level based on MOD LTP with a threshold 0.01 are shown in Fig. 7.

The accuracy of the method is tested on a simulated T2-weighted brain dataset (1 mm thickness, 0% noise and 0% intensity non-uniformity; http://www.bic.mni.mcgill.ca/brainweb). The MOD-LTP image is formed using (1) and (2) corresponding to different user-specified thresholds after normalizing the image in the range [−1 1]. As discussed in section II, the moment features are extracted from MOD-LTP and the average rank and accuracy are calculated. The traditional LBP is compared with iterated and weighted moments of MOD-LTP with a threshold 0.2. It is observed that MOD-LTP

Downloaded from http://comjnl.oxfordjournals.org/ by guest on October 14, 2014

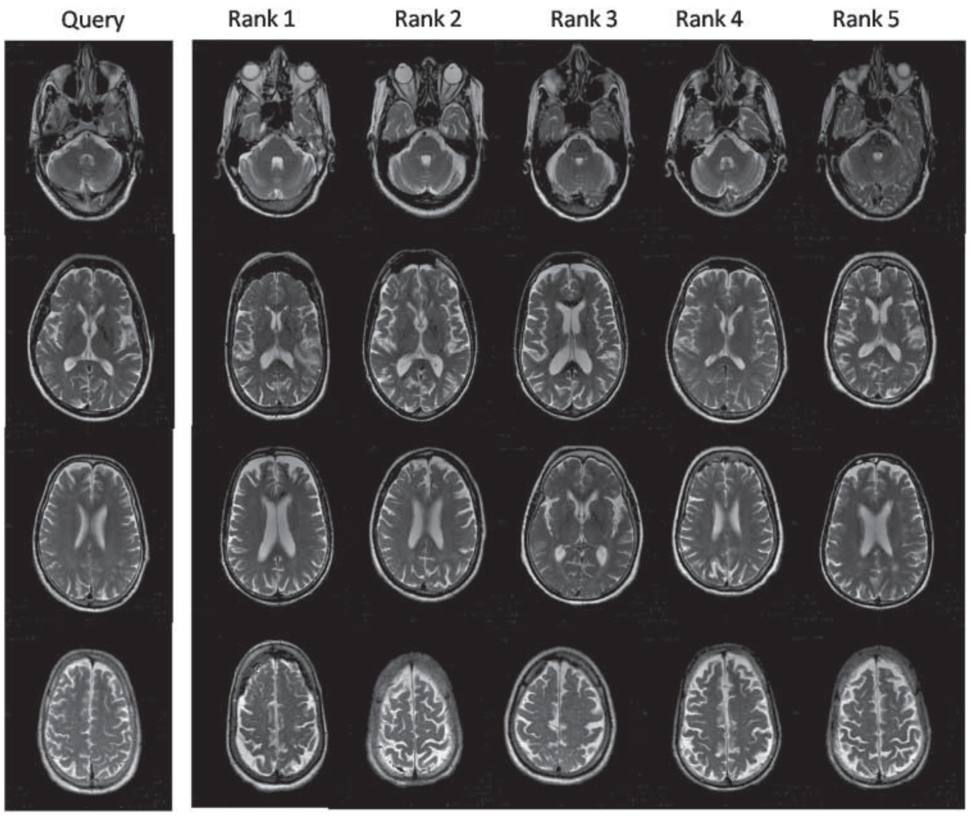

FIGURE 7. The first five images retrieved from each class.

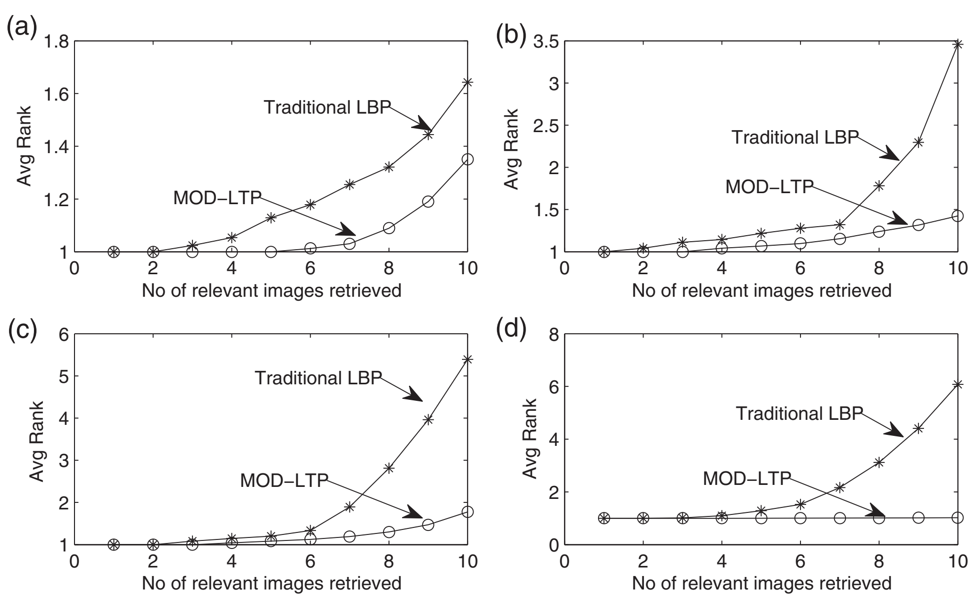

FIGURE 8. The average rank of retrieving 10 relevant images in different levels based on traditional LBP and iterated and weighted Moments of MOD-LTP with threshold 0.2 and windowsize 3. (**a**) L1, (**b**) L2, (**c**) L3, (**d**) L4.

Downloaded from http://comjnl.oxfordjournals.org/ by guest on October 14, 2014

is better than traditional LBP in terms of average rank for retrieving the first 10 relevant images. The comparison is given in Fig. 8.

The average ranks for retrieving 10 relevant images using moment features of MOD-LTP are 1.35 in Ll, 1.42 in L2, 1.77 in L3 and 1.02 in L4, while those of histogram-based traditional LBP are 1.55 in Ll, 3.4 in L2, 5.39 in L3 and 6.07 in L4. Figure 8 shows that the average rank using moment features of MOD-LTP is 1.15 times better than traditional LBP in L1, 2 times better in L2, 3 times better in L3 and 5.9 times better in L4.

LBP is sensitive to noise due to blind thresholding, but by the choice of proper threshold, sensitivity to noise in uniform region or near uniform can be reduced. This has been tested with different noise levels (1, 3, 5 and 7%). The input SNR is calculated using the equation

$$\mathrm{ISNR} = 10\log_{10}\left[\frac{\sum I_{\mathrm{org}}^2}{\sum\left(I_{\mathrm{noisy}} - I_{\mathrm{org}}\right)^2}\right], \quad (12)$$

where I_{org} is the original image and I_{noisy} is the image with various noise levels. The output SNR is calculated using the equation

$$\mathrm{FSNR} = 10\log_{10}\left[\frac{\sum I_{\mathrm{Filt}}^2}{\sum\left(I_{\mathrm{noisy}} - I_{\mathrm{Filt}}\right)^2}\right], \quad (13)$$

where I_{Filt} is the filtered image obtained using either MOD-LBP or MOD-LTP. The SNRs of MOD-LTP and MOD-LBP over various noise levels are shown in Fig. 9.

The SNR of MOD-LTP (20 db) is more than that of MOD-LBP (5.6 db) in the presence of 1% noise. The SNR of MOD-LTP becomes closer to that of MOD-LBP when the noise level present in the image is above 9%. The SNRs of MOD-LTP over different user-specified thresholds are shown in Fig. 10. It is seen that the SNR is high when the user-specified threshold is in the range from 0.24 to 0.36 for all levels.

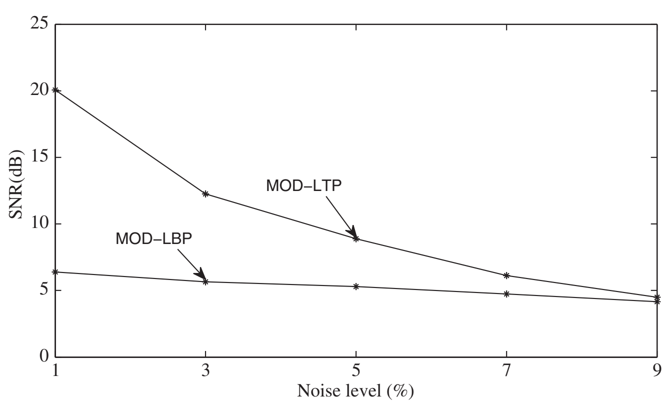

FIGURE 9. The SNR vs. noise level of MOD-LBP and MOD-LTP.

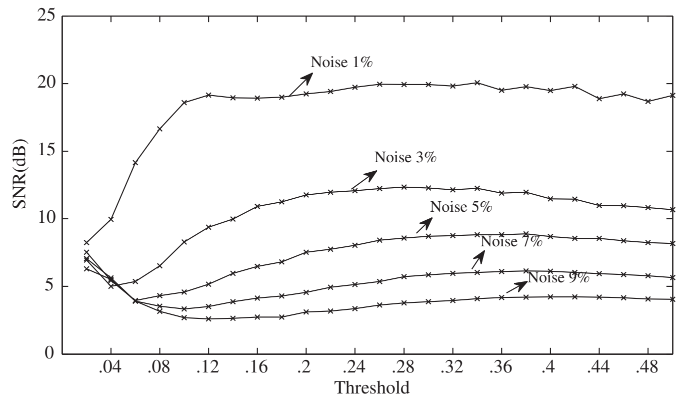

FIGURE 10. SNR vs. threshold of MOD-LTP over various noise levels.

5. CONCLUSION

This paper illustrates a method to locate relevant slices from the MR image database. The observations reveal that local structure is not affected much by intensity variations and MOD-LTP with a local variance-based threshold is robust to global illumination changes. The reweighting on moment features leads to an increase in precision for each iteration, reaching an optimal value following a few initial iterations as dependent on the class. The average precision obtained after applying the reweighting procedure is greater than that obtained with the individual features, thereby making the retrieval attempts using the individual features redundant. It shows that the MOD-LTP with a proper choice of threshold is more discriminant and less sensitive to noise in uniform or near-uniform regions. The MOD-LTP, invariant to monotonic gray-level change and rotation with respect to the window chosen, along with translation and scaling invariant central moments are very useful in identifying similar slices because of the variability in the orientation of anatomical structures within the brain across different subjects.

REFERENCES

[1] Smeulders, A.W.M., Worring, M., Santini, S., Gupta, A. and Jain, R. (2000) Content-based image retrieval at the end of the early years. *IEEE Trans. Pattern Anal. Mach. Intell.*, **22**, 1349–1380.

[2] Liu, Y., Zhang, D., Lu, G. and Ma, W.-Y. (2007) A survey of content-based image retrieval with high-level semantics. *Pattern Recognit.*, **40**, 262–282.

[3] Datta, R., Joshi, D., Li, J. and Wang, J.Z. (2008) Image retrieval ideas, influences, and trends of the new age. *ACM Comput. Surv.*, **40**, 1–60.

[4] Muller, H., Michoux, N., Bandon, D. and Geisbuhler, A. (2004) A review content-based image retrieval systems in medical applications clinical benefits and future directions. *Int. J. Med. Inform.*, **73**, 1–23.

Downloaded from http://comjnl.oxfordjournals.org/ by guest on October 14, 2014

[5] Unay, D., Ekin, A. and Jasinschi, R.S. (2010) Local structure-based region-of-interest retrieval in brain MR images. *IEEE Trans. Inf. Technol. Biomed.*, **14**, 897–903.

[6] Nanni, L. and Lumini, A. (2008) Local binary patterns for a hybrid fingerprint matcher. *Pattern Recognit.*, **41**, 3461–3466.

[7] Ojala, T., Pietikainen, M. and Harwood, D. (1996) A comparative study of texture measures with classification based on featured distribution. *Pattern Recognit.*, **29**, 51–59.

[8] Korn, P., Sidiropoulos, N., Faloutsos, C., Siegel, E. and Protopapas, Z. (1998) Fast and effective retrieval of medical tumor shapes. *IEEE Trans. Knowl. Data Eng.*, 10, 889–904.

[9] Gunaratne, P. and Sato, Y. (2003) Estimation of asymmetry in facial actions for the analysis of motion dysfunction due to paralysis. *Int. J. Image Graph.*, **3**, 639–652.

[10] Heikkila, M., Pietikainen, M. and Schmid, C. (2009) Description of interest regions with local binary patterns. *Pattern Recognit.*, **42**, 425–436.

[11] Hafiane, A., Seetharaman, G., Palaniappan, K. and Zavidovique, B. (2008) Rotationally invariant hashing of median binary patterns for texture classification. *Int. Conf. on Image Analysis and Recognition*, Lecture Notes in Computer Science 5112, portugal, June 25–27, pp. 619–629.

[12] Liao, S. and Chung, A.C.S. (2007) Face Recognition by Using Elongated Local Binary Patterns with Average Maximum Distance Gradient Magnitude. *Proc. 8th Asian Conference on Computer Vision (ACCV 2007)*, Tokyo, Japan, November 18–22, pp. 672–679.

[13] Ojala, T., Pietikainen, M. and Maeenpaa, T. (2002) Multiresolution gray-scale and rotation invariant texture classification with local binary patterns. *IEEE Trans. Pattern Anal. Mach. Intell.*, **24**, 971–987.

[14] Tan, X. and Triggs, B. (2007) Enhanced Local Texture Feature Sets for Face Recognition Under Difficult Lighting Conditions. *3rd Int. Workshop Analysis and Modelling of Faces and Gestures*, Lecture Notes in Computer Science 4778, Brazil, October 20, pp. 168–182.

[15] Ahonen, T. and Pietikainen, M. (2007) Soft Histograms for Local Binary Patterns. *Proc. Finnish signal Processing Symposium (FINSIG 2007)*, Oulu, Finland, pp. 1–4.

[16] Nanni, L., Lumini, A. and Brahnam, S. (2010) Local binary patterns variants as texture descriptors for medical image analysis. *Artif. Intell. Med.*, **49**, 117–1125.

[17] Unay, D., Ekin, A., Cetin, M., Jasinschi, R. and Erci, A. (2007) Robustness of Local Binary Patterns in Brain MR Image Analysis. *Proc. 29th Annual Int. Conf. of the IEEE EMBS Cité Internationale*, Lyon, France, August 23–26, pp. 2098–2101.

[18] Varghese, A., Kannan, B., Varghese, R.R. and Paul, J.S. (2012) Level Identification of Brain MR Images using Histogram of a LBP variant. *IEEE Conf. on Computational Intelligence and Computing Research*, Coimbatore, India, December 18–20, pp. 207–210, ISBN:978-1-4673-2481-6.

[19] Hu, M.K. (1962) Visual pattern recognition by moment invariants. *IRE Trans. Inf. Theory.*, **IT-8**, 179–187.

[20] Robert, S. (1989) *Digital Image Processing and Computer Vision*. John Wiley & Sons, Inc, NewYork.

[21] Zhang, J. and Ye, L. (2007) An Unified Framework Based on p-Norm for Feature aggregation in Content-Based Image Retrieval. *9th IEEE Int. Symp. on Multimedia*, Taichung, Taiwan, pp. 195–201.

[22] Muller, H. and Muller, W. (2001) Automated Benchmarking in Content Based Image Retrieval, Work Supported by Swiss National Foundation for Scientific Research (grant no. 2000-052426.97).

Downloaded from http://comjnl.oxfordjournals.org/ by guest on October 14, 2014